
Article:
Mackie, A.J., Dean, J.S. orcid.org/0000-0001-7234-1822 and Goodall, R. (2019) Material and magnetic properties of Sm2(Co, Fe, Cu, Zr)17permanentmagnets processed by Spark Plasma Sintering. Journal of Alloys and Compounds, 770. pp. 765-770. ISSN 0925-8388

https://doi.org/10.1016/j.jallcom.2018.08.186

Journal of Alloys and Compounds 770 (2019) 765–770

Contents lists available at ScienceDirect

Journal of Alloys and Compounds

journal homepage: http://www.elsevier.com/locate/jalcom

Material and magnetic properties of $Sm_2(Co, Fe, Cu, Zr)_{17}$ permanent magnets processed by Spark Plasma Sintering

Alexander J. Mackie*, Julian S. Dean, Russell Goodall

Materials Science and Engineering, Sir Robert Hadfield Building, Mappin Street, Sheffield, S1 3JD, UK

ARTICLE INFO

Article history:
Received 10 July 2018
Accepted 18 August 2018
Available online 21 August 2018

Keywords:
Spark plasma sintering (SPS)
Field-assisted sintering technique (FAST)
Powder processing
$Sm_2(Co$
Fe
Cu
$Zr)_{17}$
Rare earth alloys and compounds
Magnetic materials
Permanent magnets
Intermetallics
Permanent magnets
Rare earth alloys and compounds
Powder metallurgy
Magnetisation
Magnetic measurements

ABSTRACT

Improvements to the properties of Rare Earth Permanent Magnets (REPMs) are needed to advance the capabilities of electric motors and generators, and refinement of the microstructure by the use of different approaches to processing may be a key means to achieving this. We report here a systematic study into the use of Spark Plasma Sintering to process $Sm_2(Co, Fe, Cu, Zr)_{17}$ permanent magnets. This unfamiliar method for $Sm_2(Co, Fe, Cu, Zr)_{17}$ offers the potential for efficiency savings in reduced processing temperatures and times versus the industry standard vacuum sinter powder metallurgical route, and also offers a refined microstructure of the materials produced. The optimised processing conditions for achieving near-to-theoretical density are reported, and the microstructure and magnetic properties of the materials produced are compared with conventional vacuum sintering. The results provide a basis for further optimisation of these materials.

1. Introduction

Rare earth permanent magnets (REPMs), such as Nd-Fe-B and $Sm_2(Co, Fe, Cu, Zr)_{17}$, are critical components in applications such as generators for the electric grid (especially in the use of renewable energy), and electric motors with the expanding electrification of transport. To meet the growing global energy demand, there is a continuing drive to improve on key magnetic properties; remanence, coercivity and the figure-of-merit energy product, as well as minimising losses within the magnet during use. To meet these engineering challenges, an optimisation and homogenisation of the magnetic material microstructure [1] can be met with exploration of novel processing techniques, which may also bring efficiency in energy use and material usage.

One candidate technology; Spark Plasma Sintering (SPS, also called Field Assisted Sintering Technology, FAST) is a powder processing technique for metals and ceramics which utilises electric current to generate heat within an electrically conductive die (normally graphite) and between powder particles. The direct application of heat to the powders, allow very large heating rates to be achieved, especially in comparison to furnace methods which rely on in-direct heating. With the assistance of an applied uniaxial pressure, the SPS technique can sinter materials at lower temperatures [2–6] and to a high dimensional tolerance in under 30 min, compared to hours for conventional vacuum furnace sinter techniques. The shorter, more efficient processing cycles also reduce energy costs [7]. A comprehensive review of the SPS technique and the properties of materials studied is provided by Orrù et al. [8], and more recently Guillon et al. [9].

Short processing cycles and lower sinter temperatures are conduit to achieving fine-grain microstructures in permanent magnets [10–16] and the magnet's resistance to demagnetisation

* Corresponding author. University of Sheffield AMRC with Boeing, Factory of the Future, Wallis Way, S6 5TZ, UK.
E-mail address: a.mackie@sheffield.ac.uk (A.J. Mackie).

https://doi.org/10.1016/j.jallcom.2018.08.186

(coercivity) generally increases with decreasing grain size [17]. However, achieving nanoscale microstructures require fine milled powders and add additional processing steps and control implementation; with issues concerning oxidation and contamination. Few studies have been conducted utilising SPS for microcrystalline REPM powders. Microcrystalline Nd-Fe-B-type magnets processed by SPS measured magnetic properties comparable to those from conventional sinter methods, but were also shown to possess improved mechanical properties and increased corrosion and oxidation resistance [6,18–20]. Several reports also noted SPS processed materials possessed notably 'cleaner' grain boundaries; free of contaminants [5,21,22]. Uniform and homogeneous microstructures improve the resistance to demagnetisation and the overall life-cycle of REPMs operating in demanding environments, such as those utilised in the aerospace and defence fields [23].

Sm_2(Co, Fe, Cu, Zr)$_{17}$-type permanent magnets are typically processed from microcrystalline powders by a vacuum sinter method. The consolidated Sm_2(Co, Fe, Cu, Zr)$_{17}$ material then develop their magnetic properties (specifically; coercivity) only after a multi-stage, prolonged heat treatment process. The heat treatment precipitates a nanoscale cellular structure within grains, which pin domain walls and resist demagnetisation even at temperatures beyond 200 °C [24], and as a result their use is primarily in aerospace and military applications with demanding environments. Unlike other REPM materials, Sm_2(Co, Fe, Cu, Zr)$_{17}$ magnet development is not driven towards achieving nanocrystalline grain size, but instead through homogenising the microcrystalline microstructure and developing the heat treatment. Optimising the microstructure in advance of post-processing could improve the quality and effectiveness of the precipitated cellular nanostructure within the grains, which is generated during a heat treatment which can last in excess of 24 h [25].

There has been little exploration of microcrystalline Sm_2(Co, Fe, Cu, Zr)$_{17}$-type permanent magnets processed by the SPS technique. Matsumoto et al. [4] performed a study of the relative density of Sm_2(Co, Fe, Cu, Zr)$_{17}$ specimens processed by SPS in comparison to conventional sinter method specimens. They found the SPS processed specimens were able to achieve near-theoretical density for hold temperatures of 950 °C and studied pressures ranging from 39–100 MPa, compared to sintering temperatures in excess of 1400 °C for vacuum sintering method. However, there was no report on the magnetic properties. Other studies have thus far concentrated on major questions of process viability, such as the uptake of carbon (particularly deleterious to the magnetic properties of Sm_2(Co, Fe, Cu, Zr)$_{17}$) from the graphite mould during processing [26]. The adoption of the SPS technique with other REPM materials have produced permanent magnets with unique material and magnetic properties. As such, this work explores the unfamiliar processing of microcrystalline Sm_2(Co, Fe, Cu, Zr)$_{17}$ with SPS, and provides a detailed investigation of the processing parameters, the microstructure and the magnetic properties.

2. Material and experimental methods

RECOMA® 35E (Arnold Magnetic Technologies, Switzerland) commercial grade Sm_2(Co, Fe, Cu, Zr)$_{17}$ powders, produced by jet-milling and designed for high room temperature coercivity, were processed using an FCT Systeme GmbH (Frankenblick, Germany) SPS furnace, type HP D 25. A practical description of the SPS apparatus is provided by Garay [2] and the powder preparation methodology used in this work for 20 mm diameter specimens is given by Mackie et al. [26]. Isotropic Sm_2(Co, Fe, Cu, Zr)$_{17}$ specimens of the same material and processed by conventional, vacuum sintering route (labelled to as conventional sinter or CS) were produced and provided by Arnold Magnetic Technologies.

Fig. 1 displays the main processing variables of the SPS technique: Heating Rate (HR) [A], Hold Temperature (HT) [B], Hold Pressure (HP) [C]. The dwell time is defined by the length of time between the dashed lines. After the dwell period, the specimens were rapidly cooled to room temperature via removal of the applied current and contact with water cooled pistons, with the cooling rate fixed at around 100 °C\min.

As sintering is a thermally-activated process, the processing variables; HR and HT, were expected to have the largest effect on the consolidation of the Sm_2(Co, Fe, Cu, Zr)$_{17}$ powders, and as such were the focus of the initial parameter study. The non-thermal processing variables; HP and dwell time, were maintained as constants throughout the investigation. The HP used (51 MPa) was the maximum value specified for the high density graphite mould (material grade 2333, produced by Mersen, UK) and the dwell time (5 min) was selected to allow the specimen to achieve thermal homogeneity. The range of HTs studied were from 800 °C to 1100 °C and HRs between 50, 100 and 200 °C/min. The effectiveness of the processing parameters was defined by the removal of porosity and therefore determined by measurement of specimen density. This was done using an Archimedes' water immersion method with a commercial Mettler Toledo MS-DNY-43 and repeated three times to derive an average.

The heat treatment used for the SPS processed Sm_2(Co, Fe, Cu, Zr)$_{17}$ magnets comprised of homogenisation at 1070 °C in an argon atmosphere for 2 h, before allowing to cool to room temperature. An annealing stage followed at 850 °C in an argon atmosphere for 8 h, before slow cooling in an argon atmosphere at 1 °C\min to 400 °C, before quenching the specimen in oil to room temperature. Details of the heat treatment for the commercial Sm_2(Co, Fe, Cu, Zr)$_{17}$ magnet are confidential but are expected to be of a similar structure, albeit optimised to the alloy composition and processing history. Magnetic characterisation was performed using Magnet-Physik GmbH hysteresisgraph after the specimens were magnetised using a pulsed 3.5T magnetic field.

Etching of the Sm_2(Co, Fe, Cu, Zr)$_{17}$ specimens was performed using a 10% citric acid and water solution at 80 °C. Light microscopy imaging was performed using a Nikon optical microscope, SEM imaging was performed using an FEI Inspect F-50, with imaging in secondary (SE) and back-scattered (BS) modes. Particle and grain size measurements were performed using imageJ analysis software [27].

3. Results and discussion

3.1. Powder characterisation

Measurement and distributions of Sm_2(Co, Fe, Cu, Zr)$_{17}$ powders

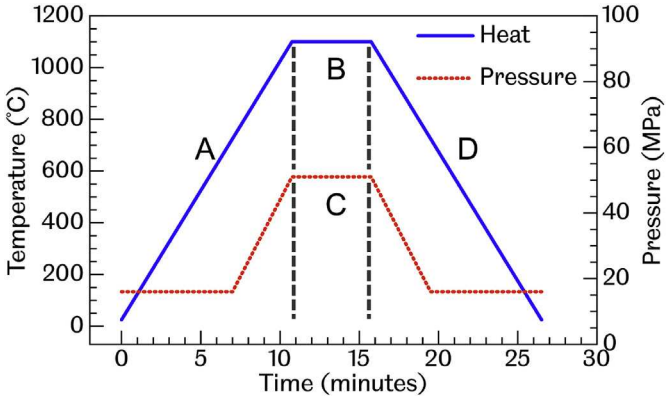

Fig. 1. Schematic detailing a typical example SPS processing scheme.

were performed for a sample of 150 random crystallites, in micrographs of which Fig. 2 was typical. The long axis diameter, a, for each crystallite was first inferred and measured, and perpendicular to this axis the short axis diameter, b, was measured. An example of these axes for a $Sm_2(Co, Fe, Cu, Zr)_{17}$ powder crystallite is shown in Fig. 2. The long and short axis diameters were also used to calculate the aspect ratio (a/b) for each crystallite, which provides an approximate quantification of crystallite geometry. Fig. 3 shows the distribution of the crystallite diameters measured and the corresponding distribution of aspect ratios. The long axis shows a main peak around 5 μm, with a smaller peak at 15 μm. The short axis distribution shows only a single peak centred around 3 μm. The aspect ratio is also bimodal, with a main peak at 1.5 and a smaller peak at 5, reflecting the distribution of the long axis diameters.

The mean long axis diameter with 95% confidence limits was calculated to be 5.9 ± 0.8 μm. The mean short axis diameter was calculated as 4.2 ± 0.6 μm. The mean aspect ratio was 1.9 ± 0.2, which confirms a general, irregular shape of the $Sm_2(Co, Fe, Cu, Zr)_{17}$ crystallites. These values were calculated with a t-distribution value of 1.96 for a sample size of 150.

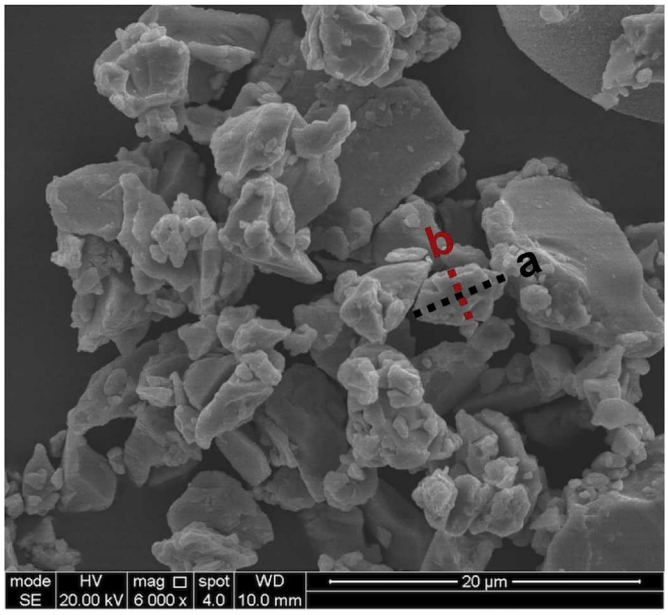

Fig. 2. SEM microscopy image of $Sm_2(Co, Fe, Cu, Zr)_{17}$ powder. Annotated axes depict long (a) and short (b) axis determined for crystallite size measurement.

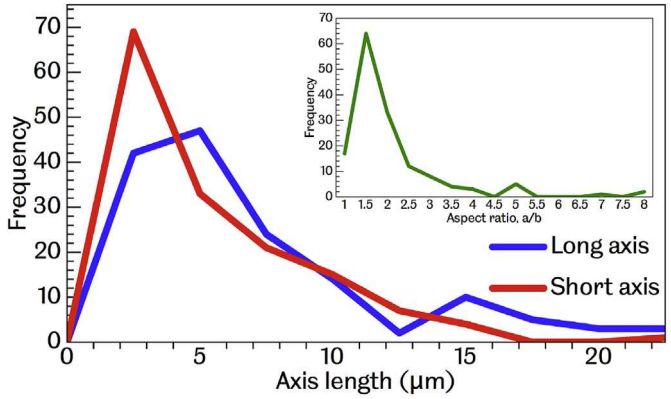

Fig. 3. Frequency distribution of long and short axes measured for 150 $Sm_2(Co, Fe, Cu, Zr)_{17}$ crystallites. Inset shows the distribution of aspect ratio for the same sample.

3.2. Processing by SPS and study of parameters

Several $Sm_2(Co, Fe, Cu, Zr)_{17}$ specimens were produced by SPS for different HT and HR as described in the methodology chapter. Their relative densities were calculated using their measured absolute density with respect to the $Sm_2(Co, Fe, Cu, Zr)_{17}$ theoretical density of 8.4 g/cm^3 [28].

The data in Fig. 4 shows the strong influence of the HT on the densification of $Sm_2(Co, Fe, Cu, Zr)_{17}$. For a HT of 800 °C, the relative density of the specimen was very low and no significant effect was observed when the HR is increased from 100 °C/min to 200 °C/min. The high porosity of these specimens increased the variability in the mass measurement when immersed in water, thus leading to increased uncertainty in the calculated density via the Archimedes' method. Increasing the HT to 1000 °C improved the density of the $Sm_2(Co, Fe, Cu, Zr)_{17}$ specimens noticeably to around 90% relative to the theoretical. A decrease in the relative density was observed as the HR was increased from 50 °C/min to 100 °C/min and 200 °C/min. When using a low HR, the overall processing cycle time is longer (even though the dwell time is fixed), therefore allowing more time for sintering to continue at a HT where the dominant sintering mechanisms do not allow full density to be reached.

For the HT of 1050 °C, high levels of densification are again achieved, although the trend with increasing HR is different than before. Here, an increase in the HR from 50 °C/min to 100 °C/min improved the final relative density of the consolidated specimens from 94.1% to 99.1%, and a similar density is achieved using 200 °C/min. This can be explained as 1050 °C is the critical temperature for sintering to occur for $Sm_2(Co, Fe, Cu, Zr)_{17}$ under the SPS HP and dwell time used in this study. Therefore, when processing at higher HR, a smaller fraction of the processing cycle was spent at lower temperatures where non-densifying mass transfer mechanisms dominate. While not bringing particle centres closer, the surface mass transfer mechanisms also reduce the pore surface curvatures and lower the driving force for densifying mass transfer mechanisms at higher temperatures. A significant enhancement in the densification for alumina was reported by Zhou et al. when the HR increased from 50 °C\min to 300 °C\min for a HT of 1150 °C [29]. However, utilising high heating rates must be balanced with sufficiently large HTs and dwell times to allow the temperature over the entire specimen to homogenise such that removal of porosity can occur throughout the entire material volume [30].

At 1100 °C, all the analysed specimens were able to achieve full densification; 99.8%, 99.4% and 99.8% relative densities were measured across the increasing heating rates studied. Regardless of how quickly the HT is reached, the $Sm_2(Co, Fe, Cu, Zr)_{17}$ specimens were able to achieve full density when using a HT of 1100 °C for

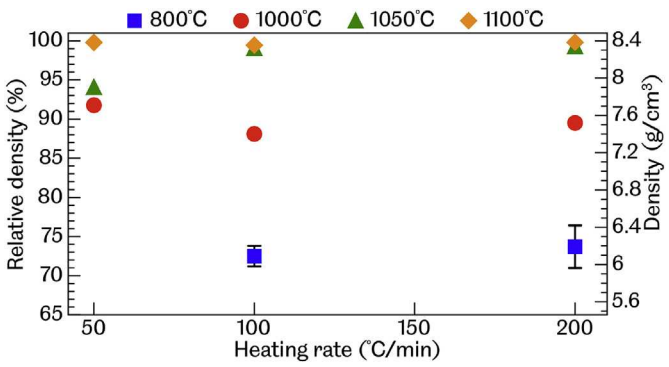

Fig. 4. Relative and absolute density of $Sm_2(Co, Fe, Cu, Zr)_{17}$ specimens after processing with different HRs and HTs by SPS technique for 5 min using HP of 51 MPa.

5 min at a maximum applied pressure of 51 MPa. Similar observations were made in the study of a range of titanium alloys. When the HT was sufficiently large, all specimens achieved full densification regardless of the HR [31]. These results were also consistent with studies of the HR on alumina powders above 1200 °C [29,32].

The SPS processing parameters; HT and HR, were both shown to have a noticeable effect on the densification of the $Sm_2(Co, Fe, Cu, Zr)_{17}$ powders. HT in particular was strongly linked to the achievable final density of the specimen, with density approximately reaching the theoretical density for $Sm_2(Co, Fe, Cu, Zr)_{17}$ at hold temperatures of 1050 °C and above. Diffusion processes are crucial to the sinter process, and the mass transfer mechanisms that facilitate densification are high energy and activated at higher temperatures. For a fixed maximum applied pressure of 51 MPa, the activation of these densification mechanisms becomes significant at around 1050 °C.

3.3. Grain size analysis

In the following subsections, an analysis of the material and magnetic properties of an optimally SPS processed and heat treated isotropic $Sm_2(Co, Fe, Cu, Zr)_{17}$ is provided. The processing parameters for this magnet were 1100 °C HT, 100 °C\min HR, 51 MPa HP and 5 min hold time. The etched microstructure of this specimen is displayed in Fig. 5.

The microstructure shows $Sm_2(Co, Fe, Cu, Zr)_{17}$ grains and samarium and oxygen-rich grain boundary precipitate features. The microstructure was homogeneous throughout, with no distinction at the surface or within the specimen centre. To measure average grain diameters, a linear intercept method [33] was used in the horizontal and vertical axis of the image and averaged. For each measurement direction, twenty lines across two microscopy images similar to Fig. 5 of the same etched specimen were used to measure grain diameters. The mean grain diameter, with 95% confidence limit, was 8.5 ± 0.3 μm. The uncertainty in these values were calculated using a t-distribution value of 2. Compared to the powder crystallites, the SPS processed $Sm_2(Co, Fe, Cu, Zr)_{17}$ magnet shows some coarsening of the granular structure. While an alternative method was used to measure the $Sm_2(Co, Fe, Cu, Zr)_{17}$ powders, the long axis diameter, 5.9 ± 0.8 μm, can effectively be used as an upper bound estimation.

For comparison, the microstructure of the conventional vacuum sinter processed and heat treated $Sm_2(Co, Fe, Cu, Zr)_{17}$ magnet is shown in Fig. 6. Here, dark-field imaging was able to be used to further highlight the grain boundaries. It can be seen that a similar microstructure and grain boundary features are observed, as in the SPS processed sample. The average grain size in Fig. 6 was measured using the same linear intercept method as previously described for the SPS processed specimen. The analysis of the microstructure shows the average grain diameter to be 54.3 ± 2.4 μm, using a t-value of 2.15 to calculate the 95% confidence value, which is significantly larger than the average grain size in the specimen produced by the SPS process. These results are in agreement with the observations made by Matsumoto et al. [4]. These results show that the SPS technique produces a finer granular microstructure for microcrystalline powders, while also achieving near-theoretical density in shorter processing cycles compared to vacuum sinter methods.

3.4. Magnetic characterisation

Key magnetic properties can be deduced from the magnetisation and subsequent demagnetisation of permanent magnets. Fig. 7 displays the demagnetisation curves for the SPS processed isotropic $Sm_2(Co, Fe, Cu, Zr)_{17}$ magnet, before and after heat treatment, as well as the commercial isotropic $Sm_2(Co, Fe, Cu, Zr)_{17}$ magnet after heat treatment.

The magnetic properties for the $Sm_2(Co, Fe, Cu, Zr)_{17}$ magnet after processing by SPS are underdeveloped, but typical for the as-cast/processed state [34,35]. After the heat treatment, both the

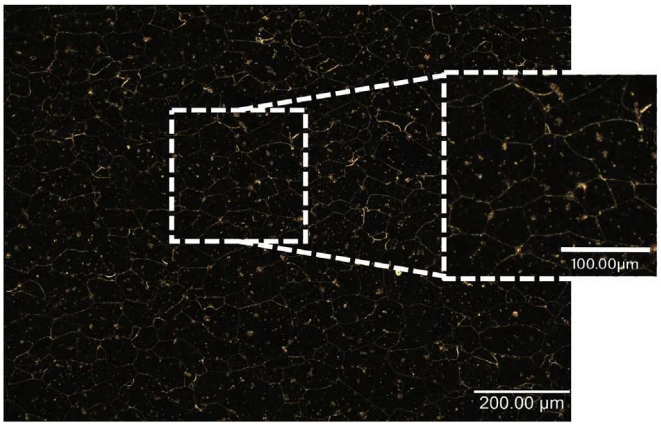

Fig. 6. Light microscopy image of citric acid etched (10% solution with water at 80 °C) $Sm_2(Co, Fe, Cu, Zr)_{17}$ processed by CS method. Grain boundaries have been emphasised by imaging in dark-field imaging mode. Inset shows magnified region for clarity.

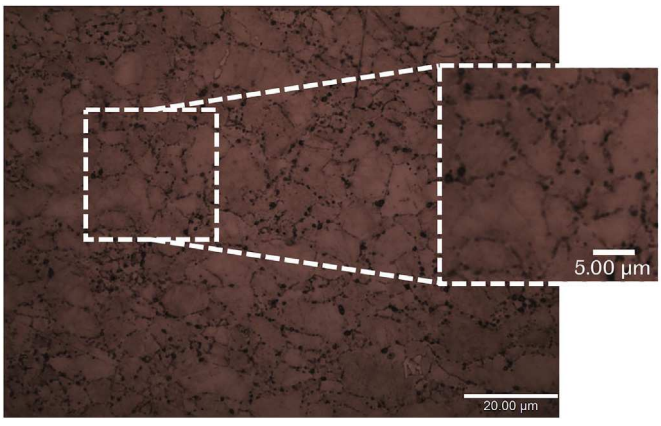

Fig. 5. Light microscopy image of citric acid etched (10% solution with water at 80 °C) $Sm_2(Co, Fe, Cu, Zr)_{17}$ processed by SPS. Inset shows magnified region for clarity.

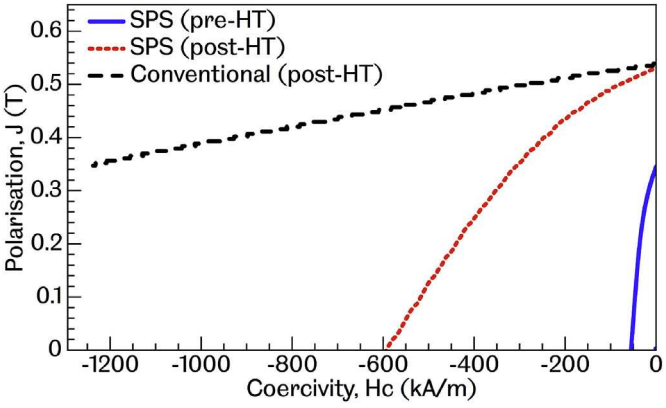

Fig. 7. Demagnetisation curves for the isotropic SPS processed $Sm_2(Co, Fe, Cu, Zr)_{17}$ magnet before and after heat treatment and the isotropic commercial $Sm_2(Co, Fe, Cu, Zr)_{17}$ magnet.

Table 1
Magnetic properties of $Sm_2(Co, Fe, Cu, Zr)_{17}$ magnets after processing by SPS and by conventional sinter (CS) method, followed by a heat treatment.

$Sm_2(Co, Fe, Cu, Zr)_{17}$ processing method	Density (g/cm^3)	Relative density (% relative to theoretical density of 8.4 g/cm^3	Remanent polarisation, J_r (T)	Intrinsic coercivity, $_JH_c$ (kA/m)	Coercive force, $_BH_c$ (kA/m)	Energy product, $(BH)_{max}$ (kJ/m^3)
SPS	8.35 ± 0.02	99.4 ± 0.2	0.37 ± 0.02	66.80 ± 3.44	60.20 ± 3.01	7.10 ± 0.36
SPS and heat treatment	8.39 ± 0.01	99.9 ± 0.1	0.53 ± 0.03	592.00 ± 29.63	288.50 ± 14.43	42.00 ± 2.10
CS and heat treatment	8.33 ± 0.03	99.2 ± 0.4	0.56 ± 0.03	≥1214.00 ± 60.70	400.50 ± 20.00	56.00 ± 2.80

remanence and coercivity in the SPS processed $Sm_2(Co, Fe, Cu, Zr)_{17}$ magnet improved prominently; with the latter within definition of a hard magnetic material [1]. The heat treatment process is crucial to $Sm_2(Co, Fe, Cu, Zr)_{17}$ permanent magnets as it facilitates the microstructural changes within grains, which are the basis for the hard magnetic properties. The precipitation of a cellular structure, comprised of nanoscale rhombohedral 2:17 Fe-rich cells and hexagonal 1:5 Cu-rich cell boundaries, crossed with Zr rich lamellar phase [24,36], during ageing, and a redistribution of elements during slow cooling, is the basis for the coercivity and remanence enhancement respectively. In particular, the coercivity is proportional to the pinning strength of magnetic domains at the cell-cell wall boundaries [24,25,37]. The conventional sinter processed and optimally heat treated commercial $Sm_2(Co, Fe, Cu, Zr)_{17}$ magnet demonstrated the largest coercivity and was therefore the hardest to demagnetise. In fact, its coercivity exceeded the reversal field of the hysteresisgraph measurement device and therefore never crossed the x-axis.

Table 1 catalogues the remanence (remanent polarisation), J_r, intrinsic coercivity, $_JH_c$, coercive force, $_BH_c$, and energy product, $(BH)_{max}$, for these specimens. The SPS processed $Sm_2(Co, Fe, Cu, Zr)_{17}$ magnet has a similar relative density and remanence to the conventional sinter processed magnet. Both types of magnet are isotropic and have not received alignment of the magnetic powders before processing. The remanence of 0.54T is approximately half of would be expected of an anisotropic commercial $Sm_2(Co, Fe, Cu, Zr)_{17}$ permanent magnet [37,38]. Isotropic, microcrystalline magnets are approximately described by the Stoner-Wohlfarth model, where $J_r = 0.5J_s$, (J_s is the saturation polarisation and it is assumed for fully aligned anisotropic magnets $J_s \approx J_r$) [39,40].

The effects of the heat treatment were reflected through the significant increase of the coercivity from 66.8 to 592.0 kA/m in the SPS processed $Sm_2(Co, Fe, Cu, Zr)_{17}$ magnet.

There is potential to further improve the coercivity, highlighted by the coercivity achieved in the commercial and optimally heat treated $Sm_2(Co, Fe, Cu, Zr)_{17}$ magnet. Optimisation of the heat treatment applicable to SPS processed $Sm_2(Co, Fe, Cu, Zr)_{17}$ magnets will be necessary to be able to identify any clear effect from the reduced grain size on the magnetic properties of SPS processed $Sm_2(Co, Fe, Cu, Zr)_{17}$ magnets.

The residual flux and coercive force combine to give the energy product of a permanent magnet. This is an indication of the energy density of the magnet and is an important figure of merit for the commercial capabilities of permanent magnets. In comparison of the two $Sm_2(Co, Fe, Cu, Zr)_{17}$ magnets processed and heat treated by different methods, the lower coercivity of the SPS processed $Sm_2(Co, Fe, Cu, Zr)_{17}$ magnet inevitably results in a lower $(BH)_{max}$ for the SPS processed magnet. It is also worth noting, for both magnets studied, the energy product can be greatly improved if alignment of the magnetic powder particles using a magnetic field was performed prior to processing. Alternatively, texture could be induced using a hot deformation process after the SPS process [15,41]. Introducing alignment or texture of the magnetic grains, as well as optimising the heat treatment process, are processing steps which would significantly enhance the energy density for $Sm_2(Co, Fe, Cu, Zr)_{17}$ magnets processed under the SPS parameters studied in this work.

4. Conclusions

An investigation has been performed studying the optimal SPS processing parameters required to achieve full densification for $Sm_2(Co, Fe, Cu, Zr)_{17}$ permanent magnet specimens. Particular focus has been given to the heating rate and hold temperature, with a justification given for fixing the maximum hold pressure and dwell time. Using a 20 mm diameter mould, $Sm_2(Co, Fe, Cu, Zr)_{17}$ specimens were produced by SPS with density of at least 8.32 g/cm^3 (99% relative to the theoretical density) using the following SPS processing parameters: 1050–1100 °C hold temperature, 100–200 °C/min heating rate, 51 MPa pressure, and 5-minute dwell time. These densities were comparable to the 99.2% relative density measured in a commercial $Sm_2(Co, Fe, Cu, Zr)_{17}$ sample produced by vacuum sinter method. However, the total processing cycle time using SPS was under 20 min and occurred at dwell temperatures approximately 200 °C lower than those required for the hour long processing cycles of the conventional sinter methodology. Minimal grain growth during the sinter process in the SPS processed microcrystalline material was a consequence of the lower sinter temperature and process cycle. However, until the heat treatment for the SPS processed $Sm_2(Co, Fe, Cu, Zr)_{17}$ magnets are optimised, it cannot be said whether the smaller grain size is directly responsible for the lower measured coercivity.

Hard magnetic properties were developed in the SPS processed magnets after undergoing a multi-stage heat treatment based upon commercially produced $Sm_2(Co, Fe, Cu, Zr)_{17}$ permanent magnets. The magnetic properties, particularly the coercivity, increased significantly, from 66.8 kA/m to 592 kA/m after a heat treatment. In comparison, a commercial $Sm_2(Co, Fe, Cu, Zr)_{17}$ magnet measured a coercivity of at least 1214 kA/m. With further work, it is believed an optimised heat treatment for SPS produced $Sm_2(Co, Fe, Cu, Zr)_{17}$ magnets could be established to enhance the coercivity to similar values of the commercially produced magnet. Aligning the magnetic grains before or utilising hot deformation during the SPS process are future methods which require investigation as methods to maximise the energy product and improve the potential of the SPS processed $Sm_2(Co, Fe, Cu, Zr)_{17}$ magnets.

There is much potential for $Sm_2(Co, Fe, Cu, Zr)_{17}$, and permanent magnets in general, to be processed by the SPS technique. Shorter processing cycles and finer, more uniform microstructures are some of the properties that have been demonstrated. With little precedence using the SPS technique with microcrystalline $Sm_2(Co, Fe, Cu, Zr)_{17}$ powders, the work presented in this article provides the framework for further study of particular properties and high-temperature performance of full density SPS processed $Sm_2(Co, Fe, Cu, Zr)_{17}$ permanent magnets. The SPS technique may demonstrate itself as a production method for $Sm_2(Co, Fe, Cu, Zr)_{17}$ permanent magnets with desirable properties for bespoke high-temperature applications.

Declarations of interest

None.

Acknowledgements

This work is supported by the EU-FP7 Accelerated Metallurgy Project (ACCMET, contract NMP4-LA-2011-263206)ACCMET.

One of the authors (AM) would like to acknowledge a studentship provided by THE EPSRC Centre for Doctoral Training in Advanced Metallic Systems (project EP/G036950).

References

[1] J.M.D. Coey, Advances in magnetics - hard magnetic Materials : a perspective, IEEE Trans. Magn. 47 (2011) 4671–4681.
[2] J.E. Garay, Current-activated, pressure-assisted densification of materials, Annu. Rev. Mater. Res. 40 (2010) 445–468, https://doi.org/10.1146/annurev-matsci-070909-104433.
[3] U. Anselmi-Tamburini, J.R. Groza, Critical assessment : electrical field/current application – a revolution in materials processing/sintering, Mater. Sci. Technol. 33 (2017) 1855–1862, https://doi.org/10.1080/02670836.2017.1341692.
[4] H. Matsumoto, N. Ikuta, T. Fujiwara, K. Konno, T. Nomoto, M. Matsuura, et al., Microstructures and magnetic properties of spark plasma sintered Fe–Cr–Co type and Sm2Co17 type magnets, J. Magn. Magn. Mater. (2004) 272–276, https://doi.org/10.1016/j.jmmm.2003.12.893. E1873–E1875.
[5] Z.A. Munir, U. Anselmi-Tamburini, M. Ohyanagi, The effect of electric field and pressure on the synthesis and consolidation of materials: a review of the spark plasma sintering method, J. Mater. Sci. 41 (2006) 763–777, https://doi.org/10.1007/s10853-006-6555-2.
[6] G.P. Wang, W.Q. Liu, Y.L. Huang, S.C. Ma, Z.C. Zhong, Effects of sintering temperature on the mechanical properties of sintered NdFeB permanent magnets prepared by spark plasma sintering, J. Magn. Magn. Mater. 349 (2014) 1–4, https://doi.org/10.1016/j.jmmm.2013.08.044.
[7] C. Musa, R. Licheri, A.M. Locci, R. Orrù, G. Cao, M.A. Rodriguez, et al., Energy efficiency during conventional and novel sintering processes: the case of Ti-Al2O3-TiC composites, J. Clean. Prod. 17 (2009) 877–882, https://doi.org/10.1016/j.jclepro.2009.01.012.
[8] R. Orrù, R. Licheri, A.M. Locci, A. Cincotti, G. Cao, Consolidation/synthesis of materials by electric current activated/assisted sintering, Mater. Sci. Eng. R Rep. 63 (2009) 127–287, https://doi.org/10.1016/j.mser.2008.09.003.
[9] O. Guillon, J. Gonzalez-Julian, B. Dargatz, T. Kessel, G. Schierning, J. Räthel, et al., Field-assisted sintering technology/spark plasma sintering: mechanisms, materials, and technology developments, Adv. Eng. Mater. 16 (2014) 830–849, https://doi.org/10.1002/adem.201300409.
[10] T. Saito, T. Takeuchi, H. Kageyama, Production of bulk amorphous and nanocomposite sintering method, IEEE Trans. Magn. 40 (2004) 2880–2882.
[11] H.V. Porwal, I. Chicinaş, O. Isnard, I. Ciascai, H. Chiriac, M. Lostun, Magnetic properties of nanocrystalline Ni3Fe compacts prepared by spark plasma sintering, Intermetallics 35 (2013) 98–103, https://doi.org/10.1016/j.intermet.2012.12.011.
[12] D. Zhang, M. Yue, J. Yang, G. Xu, W. Liu, J. Zhang, et al., Magnetic properties and structure of bulk nanocrystalline Sm(Co, Cu, Fe, Zr)7.6 sintered magnet, J. Appl. Phys. 105 (2009), 07A707, https://doi.org/10.1063/1.3067860.
[13] N. Lu, X. Song, X. Liu, J. Zhang, Preparation and magnetic properties of amorphous and nanocrystalline Sm2Co17 alloys, Intermetallics 18 (2010) 1180–1184, https://doi.org/10.1016/j.intermet.2010.02.034.
[14] D.T. Zhang, W.C. Lv, M. Yue, J.J. Yang, W.Q. Liu, J.X. Zhang, et al., Nanocrystalline SmCo5 magnet synthesized by spark plasma sintering, J. Appl. Phys. 107 (2010), 09A701, https://doi.org/10.1063/1.3334458.
[15] E. Castle, R. Sheridan, S. Grasso, A. Walton, M. Reece, Rapid sintering of anisotropic, nanograined Nd-Fe-B by flash-spark plasma sintering, J. Magn. Magn. Mater. 417 (2016) 279–283, https://doi.org/10.1016/j.jmmm.2016.05.067.
[16] H. Wuest, L. Bommer, T. Weissgaerber, B. Kieback, Magnetic and structural properties of spark plasma sintered nanocrystalline NdFeB-powders, J. Magn. Magn. Mater. 392 (2015) 74–78, https://doi.org/10.1016/j.jmmm.2015.05.014.
[17] J.M.D. Coey, Magnetism and Magnetic Materials, Cambridge University Press, Cambridge, United Kingdom, 2010.
[18] M. Yue, J. Zhang, Y. Xiao, G. Wang, T. Li, New kind of NdFeB magnet prepared by spark plasma sintering, IEEE Trans. Magn. 39 (2003) 3551–3553.
[19] M. Yue, J. Zhang, W. Liu, G. Wang, Chemical stability and microstructure of Nd-Fe-B magnet prepared by spark plasma sintering, J. Magn. Magn. Mater. 271 (2004) 364–368, https://doi.org/10.1016/j.jmmm.2003.10.002.
[20] W. Mo, L. Zhang, A. Shan, L. Cao, J. Wu, M. Komuro, Microstructure and magnetic properties of NdFeB magnet prepared by spark plasma sintering, Intermetallics 15 (2007) 1483–1488, https://doi.org/10.1016/j.intermet.2007.05.011.
[21] E.A. Olevsky, S. Kandukuri, L. Froyen, Consolidation enhancement in spark-plasma sintering: impact of high heating rates, J. Appl. Phys. 102 (2007), https://doi.org/10.1063/1.2822189.
[22] W. Xu, X. Song, Z. Zhang, H. Liang, Experimental and modeling studies on phase stability of nanocrystalline magnetic Sm2Co7, Mater. Sci. Eng. B 178 (2013) 971–976, https://doi.org/10.1016/j.mseb.2013.05.009.
[23] R.T. Fingers, C.S. Rubertus, Application of high temperature magnetic materials, IEEE Trans. Magn. 36 (2000) 3373–3375, https://doi.org/10.1109/20.908805.
[24] H. Kronmüller, D. Goll, Coercivity of 2:17 based permanent magnets, J. Iron Steel Res. Int. 13 (2006) 39–47, https://doi.org/10.1016/S1006-706X(08)60159-4.
[25] C. Maury, L. Rabenberg, C.H. Allibert, Genesis of the cell microstructure in the Sm(Co, Fe, Cu, Zr) permanent magnets with 2:17 type, Phys. Status Solidi. 140 (1993) 57–72, https://doi.org/10.1002/pssa.2211400104.
[26] A.J. Mackie, G.D. Hatton, H.G.C. Hamilton, J.S. Dean, R. Goodall, Carbon uptake and distribution in Spark Plasma Sintering (SPS) processed Sm(Co, Fe, Cu, Zr)z, Mater. Lett. 171 (2016) 14–17, https://doi.org/10.1016/j.matlet.2016.02.049.
[27] C.A. Schneider, W.S. Rasband, K.W. Eliceiri, NIH Image to ImageJ: 25 years of image analysis, Nat. Methods. 9 (2012) 671–675, https://doi.org/10.1038/nmeth.2089.
[28] S. Ruoho, M. Haavisto, E. Takala, T. Santa-Nokki, M. Paju, Temperature dependence of resistivity of sintered rare-earth permanent-magnet materials, IEEE Trans. Magn. 46 (2010) 15–20, https://doi.org/10.1109/TMAG.2009.2027815.
[29] Y. Zhou, K. Hirao, Y. Yamauchi, S. Kanzaki, Densification and grain growth in pulse electric current sintering of alumina, J. Eur. Ceram. Soc. 24 (2004) 3465–3470, https://doi.org/10.1016/j.jeurceramsoc.2003.10.013.
[30] Z. a. Munir, D.V. Quach, M. Ohyanagi, Electric current activation of sintering: a review of the pulsed electric current sintering process, J. Am. Ceram. Soc. 94 (2011) 1–19, https://doi.org/10.1111/j.1551-2916.2010.04210.x.
[31] N.S. Weston, F. Derguti, A. Tudball, M. Jackson, Spark plasma sintering of commercial and development titanium alloy powders, J. Mater. Sci. 50 (2015) 4860–4878, https://doi.org/10.1007/s10853-015-9029-6.
[32] Z. Shen, M. Johnsson, Z. Zhao, M. Nygren, Spark plasma sintering of alumina, J. Am. Ceram. Soc. 85 (2002) 1921–1927. http://onlinelibrary.wiley.com/doi/10.1111/j.1151-2916.2002.tb00381.x/abstract. (Accessed 21 May 2014).
[33] H. Engqvist, B. Uhrenius, Determination of the average grain size of cemented carbides, Int. J. Refract. Met. Hard Mater. 21 (2003) 31–35, https://doi.org/10.1016/S0263-4368(03)00005-2.
[34] G. Hadjipanayis, W. Tang, High temperature 2:17 magnets: relationship of magnetic properties to microstructure and processing, Magn. IEEE 36 (2000) 3382–3387, https://doi.org/10.1109/20.908808.
[35] M. Palit, D.M. Rajkumar, S. Pandian, S.V. Kamat, Effect of grain size on microstructure and magnetic properties of Sm2(Co,Cu,Fe,Zr)17 permanent magnets, Mater. Chem. Phys. 2 (2016) 1–9, https://doi.org/10.1016/j.matchemphys.2016.05.033.
[36] X. Xiong, T. Ohkubo, T. Koyama, K. Ohashi, Y. Tawara, K. Hono, The microstructure of sintered Sm(Co0.72Fe0.20Cu0.055Zr0.025)7.5 permanent magnet studied by atom probe, Acta Mater. 52 (2004) 737–748, https://doi.org/10.1016/j.actamat.2003.10.015.
[37] O. Gutfleisch, K.-H. Müller, K. Khlopkov, M. Wolf, a. Yan, R. Schäfer, et al., Evolution of magnetic domain structures and coercivity in high-performance SmCo 2:17-type permanent magnets, Acta Mater. 54 (2006) 997–1008, https://doi.org/10.1016/j.actamat.2005.10.026.
[38] J. Fidler, P. Skalicky, F. Rothwarf, High resolution electron microscope study of Sm(Co, Fe, Cu, Zr)7.5magnets, IEEE Trans. Magn. M (1983) 2041–2043.
[39] D.C. Crew, L.H. Lewis, Effect of grain alignment on magnetic structure in nanoscale material, IEEE Trans. Magn. 37 (2001) 2512–2514, https://doi.org/10.1109/20.951219.
[40] S.A. Romero, M.F. de Campos, H.R. Rechenberg, F.P. Missell, Interacting Stoner-Wohlfarth behavior in hysteresis curves of Sm(CoFeCuZr)z magnets, J. Magn. Magn. Mater. 320 (2008) 5–8, https://doi.org/10.1016/j.jmmm.2008.02.055.
[41] E. Castle, R. Sheridan, W. Zhou, S. Grasso, A. Walton, M.J. Reece, High coercivity, anisotropic, heavy rare earth-free Nd-Fe-B by flash spark plasma sintering, Sci. Rep. 7 (2017) 1–12, https://doi.org/10.1038/s41598-017-11660-9.